INTERNATIONAL JOURNAL FOR NUMERICAL METHODS IN FLUIDS VOL. 21, 183–204 (1995)

A COMPARISON OF INTEGRATION AND INTERPOLATION EULERIAN–LAGRANGIAN METHODS

ANABELA OLIVEIRA* AND ANTÓNIO M. BAPTISTA

Center for Coastal and Land-Margin Research and Department of Environmental Science and Engineering, Oregon Graduate Institute of Science & Technology, 20000 NW Walker Road, PO Box 91000, Portland, OR 97291-1000, U.S.A.

SUMMARY

Selected finite element Eulerian–Lagrangian methods for the solution of the transport equation are compared systematically in the relatively simple context of 1D, constant coefficient, conservative problems. A combination of formal analysis and numerical experimentation is used to characterize the stability and accuracy that results from alternative treatments of the concentrations at the feet of the characteristic lines. Within the methods analyzed, those that approach such treatment with the perspective of 'integration' rather than 'interpolation' tend to have superior accuracy. Exact integration leads to unconditional stability and excellent accuracy. Quadrature integration leads only to conditional stability, but newly derived criteria show that stability restrictions are relatively mild and should not preclude the usefulness of quadrature integration methods in a range of practical applications. While conclusions cannot be extended directly to multiple dimensions and complex flows and geometries, results should provide useful insight to the development and behaviour of specific Eulerian–Lagrangian transport models.

KEY WORDS: transport equation; Eulerian–Lagrangian methods; stability analysis; accuracy analysis; numerical experimentation

1. INTRODUCTION

Eulerian–Lagrangian methods (ELMs) have evolved much over the last three decades to become one of the most attractive techniques for the solution of advection-dominated transport. The basic concept of ELMs is simple: the transport equation is solved in Lagrangian form 'along' characteristic lines, effectively decoupling the advection and diffusion terms but retaining the convenience of fixed computational grids. However, there are many different ways to implement this concept and several ELMs have been proposed and applied over the years.[1–41]

As frequently happens in fast-evolving areas, much more attention has been paid to the development of new ELMs than to the systematic comparison of existing ones. Consequences include the existence of disparate terminologies and of a large number of similar but distinct techniques, whose individual and relative merits are too often misunderstood. This paper, which updates earlier systematic comparisons,[1,2] focuses on finite-element-based ELMs (FE-ELMs), a popular and fast-evolving class of methods.

FE-ELMS have been applied in many displinary areas in one, two and three dimensions.[3–10] They are generally recognized as rather attractive when advection is the dominant transport process, but questions remain about their robustness (e.g. there is no inherent mass preservation) and about which implementations are most effective. For instance, FE-ELMs that use the concept of integration (rather

* Author to whom correspondence should be addressed.

CCC 0271–2091/95/030183–22

Received 10 February 1994
Revised 12 December 1994

than interpolation) to handle the initial conditions of the diffusion step have rather promising accuracy when they are stable, but lead to instability under conditions that have not been fully understood. In order to better understand this specific problem, we step back into the relatively simplistic context of 1D, constant coefficient, non-reactive transport and use formal analysis and numerical experimentation to compare a number of 'interpolation' and 'integration' FE-ELMs and to develop criteria for their stability and accuracy.

The paper is divided into five main sections. Section 2 briefly reviews the history of the evolution of ELMs and introduces the methods selected for analysis. Out of necessity, some new nomenclature is introduced. While this nomenclature may be transitory, it creates a guiding taxonomy that helps the reader throughout the paper and addresses a growing need for systematics in numerical analysis. Section 3 provides the rationale for our choice of specific methods and describes their formulation. Additional nomenclature is introduced, completing the taxonomy adopted in the paper. Sections 4 and 5 examine, respectively, the stability and the accuracy of the selected methods, based on formal analysis of truncation and propagation errors. Error formulae are compiled in tables and errors are mapped in ways that foster the analysis of individual methods. Several numerical tests are included to provide a complementary examination of the properties of the methods. Section 6 provides an overview of the results and examines implications for future ELM research and for the ongoing development and use of a new generation of multidimensional Eulerian–Lagrangian models for environmental applications in surface waters.

2. BACKGROUND

Eulerian–Lagrangian concepts were introduced in the 1950s and 1960s through the contributions of several researchers.[11,12] In an attempt to avoid the wiggles that plague centred finite difference solutions of the advection-dominated transport equation, a Lagrangian operator was proposed,[12]

$$\frac{Dc}{Dt} \equiv \frac{\partial c}{\partial t} + u\frac{\partial c}{\partial x} = D\frac{\partial^2 c}{\partial x^2}, \tag{1}$$

using the discrete algorithm

$$\frac{c_j^{n+1} - c^{\xi}}{\Delta t} = D\frac{c_{j+1}^n - 2c_j^n + c_{j-1}^n}{\Delta x^2}, \tag{2}$$

where c is the concentration, u is the velocity and D is the diffusion coefficient. The location x^{ξ} of the foot of each backward characteristic line is obtained by integration (trivial for uniform velocities) as

$$x^{\xi} = x_j + \int_{t_{n+1}}^{t_n} u\,\mathrm{d}\tau \equiv x_j - u\Delta t \tag{3}$$

and the associated concentrations c^{ξ} are obtained by interpolation or extrapolation as

$$c^{\xi} = c_j^n + \frac{c_j^n - c_{j-1}^n}{\Delta x}(x^{\xi} - x_j). \tag{4}$$

This method effectively decouples advection from diffusion. The decoupling is physically based in the sense that it results naturally from the introduction of backward characteristic lines that follow the flow. Three distinct steps are involved in the overall solution:

(i) determination of the location of the feet of the characteristic lines
(ii) determination of the concentrations at the feet of the characteristic lines
(iii) solution of the Lagrangian form of the diffusion equation, using concentrations at the feet of the characteristic lines as initial conditions.

Both the decoupling strategy and the three generic solution steps are identifying properties of Eulerian–Lagrangian methods. However, this pioneering method had a major limitation. Indeed, the concentration at the foot of the characteristic line passing through node j at time t^{n+1} is determined from the concentrations at nodes j and $j-1$; hence for Courant numbers larger than unity this determination involves an extrapolation and the algorithm becomes unstable. Furthermore, insertion of equation (4) into equation (2) leads to

$$\frac{c_j^{n+1}-c_j^n}{\Delta t}+u\frac{c_j^n-c_{j-1}^n}{\Delta x}=D\frac{c_{j+1}^n-2c_j^n+c_{j-1}^n}{\Delta x^2}, \tag{5}$$

which shows that the advection term is effectively approximated by a conventional upwind scheme: hence the proposed method can be easily interpreted as essentially a Eulerian upwind method.

It took over a decade for the pioneering concept embodied in the work of Leith and others to lead to the truly distinctive group of methods now known as ELMs. Daubert[13] may have been the first to recognize that Courant number restrictions could be avoided by interpolating between the nodes that bound the foot of each characteristic line rather than by extrapolating from the vicinity of the head of the characteristic line. In its conceptual simplicity this recognition may qualify as the single most important development in ELM history.

Daubert also recognized that interpolating linearly to find concentrations at the feet of the characteristic lines is a major source of errors and suggested the use of quadratic interpolation. Following these early steps, the optimization of the strategy for interpolation at the feet of the characteristic lines became a focus for ELM research during the 1980s. A large number of interpolators were developed, none of which can be recognized as 'optimal' as shown by two systematic reviews.[1,2]

In conjunction with the search for optimal interpolators, the notion of using ELMs in a finite element (FE) context increased. While many FE-ELMs[3,14–16] differ 'mechanically' but not in any fundamental conceptual way from the corresponding finite difference ELMs, some[17–22] have taken advantage of the fact that, in a finite element context, the problem of 'interpolation' at the feet of the characteristic lines can effectively be expressed as an 'integration' problem.

To illustrate this point, we consider the evaluation of the contribution of a generic element k to the weak form of the weighted residual statement

$$\int_{\Omega_k}\phi_m\frac{Dc}{Dt}\,\mathrm{d}x=-D\int_{\Omega_k}\frac{\partial\phi_m}{\partial x}\frac{\partial c}{\partial x}\,\mathrm{d}x+\text{boundary terms}, \tag{6}$$

where ϕ_m are the weighting functions.

The evaluation of the integrals does not pose any problem at time $n+1$, where the derivatives of the elemental shape functions are continuous. However, integrals at time n (Figures 1(a)–1(c)) involve shape functions from more than one element; hence concentration derivatives are discontinuous over the region of integration. The form in which these discontinuities at time n are addressed provides an important distinguishing criterion among FE-ELMs.

'Interpolation FE-ELMs'[2,3] simply 'ignore' the discontinuity of ∇c. The concentrations and concentration derivatives are evaluated at the feet of the characteristic lines and assigned to a polynomial interpolation function. This interpolation function provides the basis for the integration (Figure 1(a)), which may be analytical or numerical. Comparison of alternative interpolation functions[1,2] shows that unsatisfactory compromises between cost/feasibility and accuracy become necessary and limit the implementation of the most accurate interpolation ELMs in multiple dimensions.

'Quadrature FE-ELMs'[17,18] explicitly recognizes that the operation that ultimately has to be performed is an integration and take a conceptually distinct approach: rather than tracking nodes, these

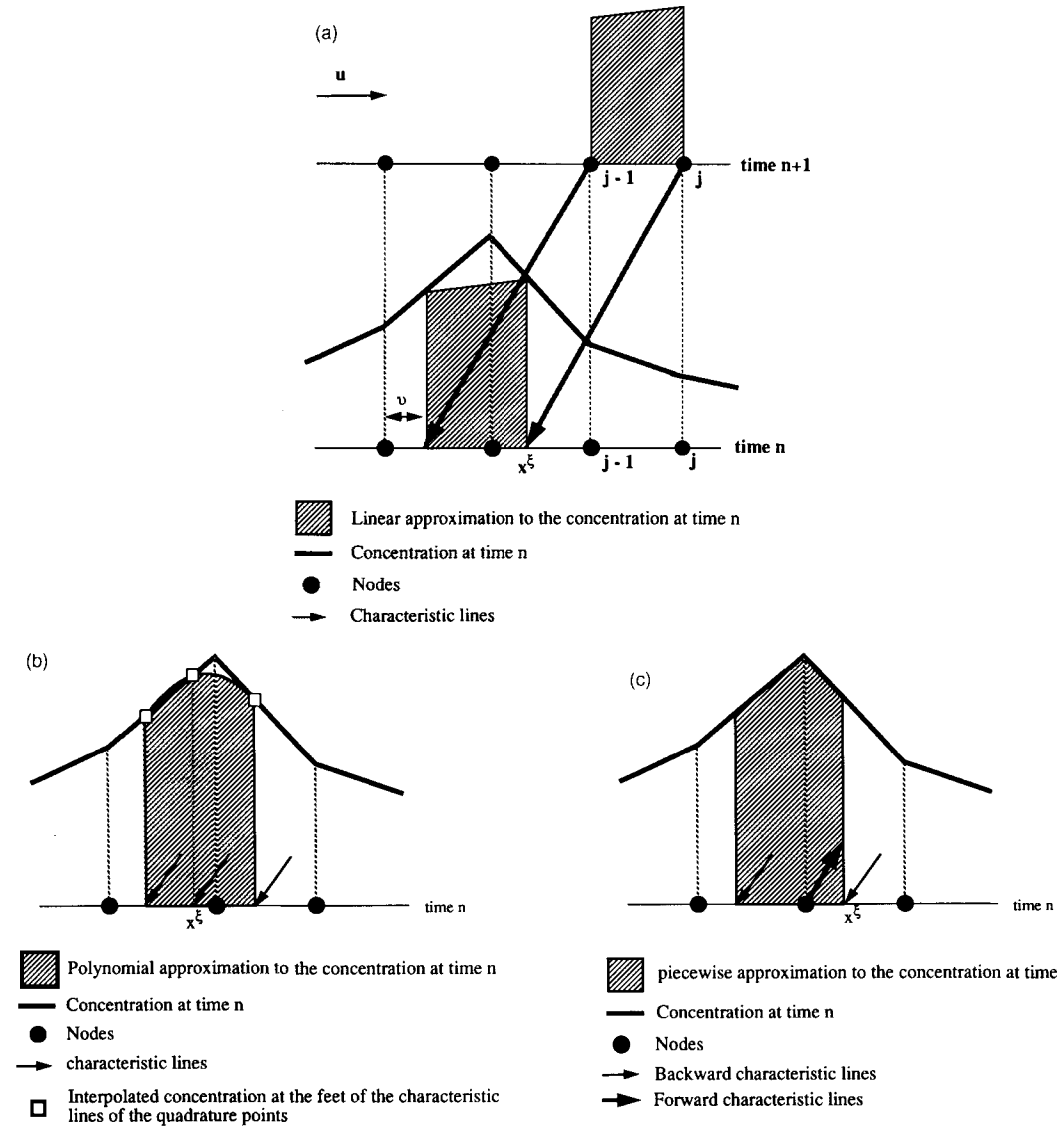

Figure 1. Approach to the evaluation of integrals at the feet of characteristic lines: (a) interpolation ELM; (b) quadrature ELM; (c) piecewise ELM

methods track quadrature points backwards from $n + 1$ (Figure 1(b)), which are then used for integration at n. Integration is now necessarily numerical and is typically based on Gauss or Lobatto quadrature. Quadrature ELMs are generally less diffusive than interpolation ELMs but are only conditionally stable, as first shown by Morton *et al.*[23] and more systematically investigated in later sections. A very attractive property of quadrature FE-ELMs is their straightforward implementation in multiple dimensions.

'Piecewise integration FE-ELMs' also recognize the key role of integraton. These methods track nodes and/or other 'notable points' both from $n + 1$ to n and from n to $n + 1$; the domain of integration is effectively divided into subdomains within which integrals can be evaluated *exactly*,

either numerically or analytically. Notable points tracked from n to $n+1$ may (Figure 1(c)) or may not correspond to discontinuities in first derivatives of concentration. The approach was introduced by Yeh *et al.*[19] borrowing some concepts from Neuman;[24] a simpler implementation is proposed in this paper.

The above three classes cover most FE-ELMs currently available. A fourth and important class, however, is constituted by the 'Eulerian–Lagrangian localized adjoint methods' (ELLAMs). The term ELLAM has evolved from the research of Russell, Celia, Herrera and co-workers,[9,20–22,25] although methods with similar characteristics were introduced earlier.[26–29] Loosely speaking, ELLAMs are FE-ELMs with weighting functions defined in the space–time domain, which are formally chosen to represent or approximate a solution of the homogeneous adjoint equation.

ELLAMs provide a formal approach to the treatment of boundary conditions and enforce global mass conservation for problems with constant coefficients.[20,21] Furthermore, ELLAMs provide a framework to interpret other classes of FE-ELMs. In particular, for constant coefficients, ELLAMs revert, in the interior of the domain, to specific forms of either interpolation or integration FE-ELMs.[20]

3. NUMERICAL FORMULATIONS

Two alternative generic ELM formulations – Galerkin ELMs and ELLAMs – are presented and customized to obtain the specific FE-ELMs compared in this paper.

3.1. *Generic formulations*

Galerkin ELM formulation. The Lagrangian form of the transport equation is discretized in time as

$$\frac{c^{n+1}-c^{\xi}}{\Delta t}-\alpha D\frac{\partial^2 c}{\partial x^2}\bigg|^{n+1}-(1-\alpha)D\frac{\partial^2 c}{\partial x^2}\bigg|^{\xi}=0, \tag{7}$$

where c^{ξ} is the concentration at the feet of the characteristic lines and $\alpha \in [0,1]$. Standard application of a weak Galerkin weighted residual finite element formulation leads to

$$\sum_{k=1}^{N_{\text{elems}}}\left(\frac{1}{\Delta t}(\Psi_{kj}^{n+1}-\Psi_{kj}^{\xi})+D[\alpha\Phi_{kj}^{n+1}+(1-\alpha)\Phi_{kj}^{\xi}]\right)+BT=0, \tag{8}$$

with

$$\Psi_{kj}^{m}=\int_{\Omega_k}c^{m}\phi_j\,\mathrm{d}x=\frac{\Delta x}{2}\int_{-1}^{1}c^{m}\phi_j\,\mathrm{d}r, \qquad \Phi_{kj}^{m}=\int_{\Omega_k}\frac{\partial c}{\partial x}\bigg|^{m}\frac{\partial \phi_j}{\partial x}\,\mathrm{d}x=\frac{2}{\Delta x}\int_{-1}^{1}\frac{\partial c}{\partial r}\bigg|^{m}\frac{\partial \phi_j}{\partial r}\,\mathrm{d}r, \tag{9}$$

where r denotes local co-ordinates, m represents either time level ξ or $n+1$ and ϕ_j are weighting functions that coincide, on an elemental basis, with the shape functions. The boundary terms (BT) are

$$BT=\left(-D\alpha\phi_j\frac{\partial c}{\partial x}\bigg|^{n+1}-D(1-\alpha)\phi_j\frac{\partial c}{\partial x}\bigg|^{\xi}\right)_{\Gamma}, \tag{10}$$

where Γ represents the boundaries.

At this stage, choices need to be made regarding (a) the location of the heads of the characteristic lines, (b) the strategy for interpolation of concentrations and concentration derivatives at ξ and (c) the strategy for evaluation of integrals at time n. Most choices will lead to finite difference analogues of

the generic form

$$\sum_{i=l_1}^{l_2} L_i c(j+i, n+1) = \sum_{i=r_1}^{r_2} H_i c(j-K+i, n), \tag{11}$$

where L_i and H_i are the coefficients associated with the concentration at time $n+1$ and node $j+1$ and the concentration at time n and node $j-K+i$ respectively. Pointers l_1, l_2, r_1 and r_2 specify the nodes involved in the contribution of the elements that contain node j to the weighted residual statement and K identifies the element that contains the foot of the characteristic line of node j.

ELLAM formulation. In contrast with Galerkin FE-ELMs, ELLAMs retain the Eulerian form of the transport equation

$$L(c) = \frac{\partial c}{\partial t} + u\frac{\partial c}{\partial x} - D\frac{\partial^2 c}{\partial x^2} = 0 \tag{12}$$

and resort to space–time weighting functions, leading to the weighted residual statement

$$\int_{t^n}^{t^{n+1}} \int_{\Omega} w_j(x, t) L(c)\, \mathrm{d}x\, \mathrm{d}t = 0. \tag{13}$$

Each weighting function w_j is defined by setting the adjoint operator L^* to zero in each element, i.e.

$$L^* = -\frac{\partial w_j}{\partial t} - u\frac{\partial w_j}{\partial x} - D\frac{\partial^2 w_j}{\partial x^2} = 0, \tag{14}$$

where L^* results naturally from the integration by parts of the original weighted residual statement

$$\int L(c) w_j \, \mathrm{d}x\, \mathrm{d}t = \int L^*(w_j) c \, \mathrm{d}x\, \mathrm{d}t + \text{boundary terms}. \tag{15}$$

Equation (14) has several solutions. To link the definition of the weighting function to the concept of characteristic lines (Figures 2(a)), we let

$$\frac{\partial w_j}{\partial t} + u\frac{\partial w_j}{\partial x} = 0, \qquad D\frac{\partial^2 w_j}{\partial x^2} = 0. \tag{16}$$

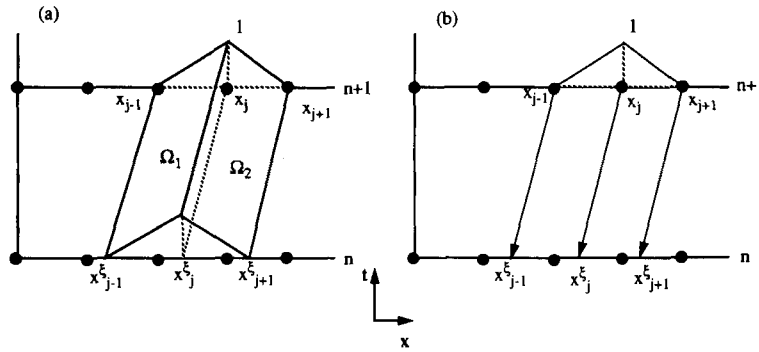

Figure 2. Comparison of weighting functions: (a) ELLAMs; (b) traditional ELMs

The weak form of equation (13) leads to

$$\sum_{k=1}^{N_{\text{elems}}} (\Psi_{kj}^{n+1} - \Psi_{kj}^{\xi} + \Phi_{kj} - \Upsilon_{kj}) + BT = 0, \tag{17}$$

with

$$\Psi_{kj}^{m} = \int_{\Omega_k} c^m w_j \, dx, \qquad \Phi_{kj} = \int_{t^n}^{t^{n+1}} \int_{\Omega_k} D \frac{\partial c}{\partial x} \frac{\partial w_j}{\partial x} \, dx \, dt, \tag{18a,b}$$

$$\Upsilon_{kj} = \int_{t^n}^{t^{n+1}} \int_{\Omega_k} c\left(\frac{\partial w_j}{\partial t} + u \frac{\partial w_j}{\partial x}\right) dx \, dt, \qquad BT = \int_{t^n}^{t^{n+1}} \left[w_j \left(uc - D \frac{\partial c}{\partial x}\right)\right]_{\Gamma} dt. \tag{19a,b}$$

Assuming exact tracking of the characteristic lines, the double integral in equation (19a) vanishes owing to equation (16). An α-method* is selected to approximate the time integration,[20] then equation (17) can be rewritten as

$$\sum_{k=1}^{N_{\text{elems}}} [\Psi_{kj}^{n+1} - \Psi_{kj}^{\xi} + \Delta t \alpha \Phi_{kj}^{n+1} + \Delta t(1-\alpha)\Phi_{kj}^{\xi}] + BT = 0, \tag{20}$$

with

$$\Phi_{kj}^{m} = \int_{\Omega_k} D \frac{\partial c}{\partial x}\bigg|^{m} \frac{\partial w_j}{\partial x} \, dx \, dt. \tag{21}$$

Comparison of equations (8) and (20) shows that within the constraints (constant coefficients, non-reactive transport) of our analysis, except for the boundary elements, the two generic formulations–ELLAMs and Galerkin FE-ELMs–differ only in the definition of the weighting functions ϕ and w. Since w is constant in time along the characteristic lines, it is enough to select the same weighting function in space for the methods to coincide.[20] For instance, the chapeau function can be used for Galerkin FE-ELMs and the 'chapeau function along the characteristics'[21] for ELLAMs (Figure 2). Therefore the analysis in the remainder of this paper is equally applicable to ELLAMs and Galerkin FE-ELMs.

3.2. *Specific formulations*

Interpolation methods. In this class of FE-ELMs the nodes at time $n+1$ are tracked backwards and the concentration and its derivative at the feet of the characteristic lines are obtained by interpolation with polynomial functions. The interpolated values are then assigned to elemental shape functions at $n+1$ to define the initial conditions for the diffusion equation.

As discussed by Baptista,[2] the polynomial functions used for interpolation at the feet of the characteristic lines may be compact (in the sense of being defined exclusively by the nodes of the element–'core' element—that contains the foot of the characteristic line, x^{ξ}) or non-compact. We will select here a non-compact cubic interpolator (4P-LR2 in Baptista's notation) that relies on information from the nodes of a linear core element and its two adjacent neighbours. The 4P-LR2 leads to an accuracy similar to that of the much more common quadratic compact interpolator[3] and has the advantage, for the purpose of the present paper, of having a linear rather than a quadratic core element.

* For an alternative approach to the time integration, involving a second application of the chain rule to equation (18b), see Reference 21.

Linear core elements lead to time-independent amplification errors and to the dominance of amplification errors over phase errors, two properties shared by all integration methods discussed in later sections.

The concentration at the feet of the characteristic lines for the 4P-LR2 is given by cubic polynomials defined by concentrations both at the nodes of the core element and at two adjacent nodes. The concentration after the interpolation step, for a generic position over the element, is defined by linear Lagrangian polynomials, i.e.

$$c^{\xi}(r) = \sum_{i=1}^{2} \phi_i c_i^{\xi} = \sum_{i=1}^{2} \phi_i \sum_{l=1}^{4} \theta_l c_{i-\operatorname{int}\beta+l-3}^{\xi}, \tag{22}$$

where c_i^{ξ} is the concentration at the foot of the characteristic line of node i, ϕ_i are the shape functions, β is the Courant number and θ_l are defined as

$$\phi_i = \begin{cases} \phi_1 = \dfrac{1}{2}(1-r), \\ \phi_2 = \dfrac{1}{2}(1+r), \end{cases} \qquad \theta_l = \begin{cases} \theta_1 = -\dfrac{1}{48}(r^3 - 3r^2 - r + 3), \\ \theta_2 = \dfrac{1}{48}(3r^3 - 3r^2 - 27r + 27), \\ \theta_3 = \dfrac{1}{18}(r^3 + r^2 - 9r - 9), \\ \theta_4 = -\dfrac{1}{48}(r^3 + 3r^2 - r - 3), \end{cases} \tag{23}$$

with $r \in [-1, 1]$ in the core element. The finite difference analogue for the 4P-LR2 is presented in Table I.

The interpolation methods can be applied either in a Galerkin FE-ELM or an ELLAM framework. In the first case the initial conditions for the diffusion step are defined over the element at time $n+1$ (equation (22)). For the ELLAM approach the concentration after advection does not need to be transported along the characteristic lines, since the weighting functions are unambiguously defined at time n (Figure 2). For constant coefficients $w_j(x, t^{n+1}) \equiv \phi_j(x)$, hence interpolation Galerkin FE-ELMs coincide with interpolation ELLAMs.

Piecewise integration methods. These methods are based on the exact evaluation of the integrals at the feet of the characteristic lines. In a Galerkin FE-ELM framework this is accomplished by following the backward tracking of the nodes (from $n+1$ to n) by a forward tracking (from n to $n+1$) of the nodes and other notable points found between two consecutive feet of the characteristic lines[19] (Figure 1(c)). As a consequence, the initial conditions for the diffusion equation have discontinuities in the first derivative within each element. In order to evaluate the integrals exactly, either numerically or analytically, elements are split into regions where the first derivatives are continuous.

In the original piecewise integration method, proposed by Yeh *et al.*,[19] the final concentration in an element is a piecewise function defined by the nodes and by the forward-tracked points (notable points). This technique is theoretically very attractive but may lead to very high computational costs, since the number of notable points necessary to define the concentration inside one element accumulates over time.

We propose a simpler implementation of the piecewise integration concept (pi-ELM) which provides a cost per time step that is independent of the duration of the simulation. The concept of notable points is eliminated and the initial conditions for the diffusion equation are solely defined by the concentration at the backward and forward-tracked nodes (Figure 1(c)). For constant velocity only one node is found between two consecutive feet of the characteristic lines, thus the concentration after

Table I. Finite difference analogues*

pi-ELM

$$\tfrac{1}{6}(c_{j-1}^{n+1}+4c_j^{n+1}+c_{j+1}^{n+1})-\alpha\boldsymbol{D}(c_{j-1}^{n+1}-2c_j^{n+1}+c_{j+1}^{n+1})$$

$$=\left[\frac{1-\upsilon}{48}\left(\frac{1}{r+1}(-2r^3-6r^2+6r-2)+3r^2+6r+3\right)+\frac{1-\upsilon}{2}\boldsymbol{D}(1-\alpha)\right]c_{j-\mathrm{int}\beta-2}^{n}$$

$$+\left[\frac{1}{24}\left(\frac{1-\upsilon}{r+1}(2r^3+3r^2-1)+\frac{1+\upsilon}{r-1}(-r^3+3r-2)+\frac{3r^2}{2}(-1+3\upsilon)+3r(1+\upsilon)\right.\right.$$

$$\left.\left.+\frac{21}{2}-\frac{15}{2}\upsilon\right)-\frac{1-\upsilon}{2}\boldsymbol{D}(1-\alpha)\right]c_{j-\mathrm{int}\beta-1}^{n}$$

$$+\left[\frac{1}{24}\left(\frac{1-\upsilon}{r+1}(-r^3+3r^2+2)+\frac{1+\upsilon}{r-1}(2r^3-3r^2+1)+\frac{3r^2}{2}(-1-3\upsilon)\right.\right.$$

$$\left.\left.+3r(-1+\upsilon)+\frac{21}{2}+\frac{15}{2}\upsilon\right)+\frac{\boldsymbol{D}(1-\alpha)}{2}(-1-3\upsilon)\right]c_{j-\mathrm{int}\beta}^{n}$$

$$+\left[\frac{1+\upsilon}{48}\left(\frac{1}{r-1}(-2r^3+6r^2-6r+2)+3r^2-6r+3\right)+\frac{1+\upsilon}{2}\boldsymbol{D}(1-\alpha)\right]c_{j-\mathrm{int}\beta+1}^{n}$$

qu-ELM

$$\tfrac{1}{6}(c_{j-1}^{n+1}+4c_j^{n+1}+c_{j+1}^{n+1})-\alpha\boldsymbol{D}(c_{j-1}^{n+1}-2c_j^{n+1}+c_{j+1}^{n+1})$$

$$=\left[\sum_{i=1}^{nqp}w_i\left(\frac{(1+r_i)(1-\upsilon_i)}{8}+\frac{(1-\alpha)\boldsymbol{D}}{2}\right)\right]c_{j-\mathrm{int}(\beta-r_i/2-0\cdot5)-2}^{n}$$

$$+\left[\sum_{i=1}^{nqp}w_i\left(\frac{(1-r_i)(1-\upsilon_i)}{8}+\frac{(1+r_i)(1+\upsilon_i)}{8}-(1-\alpha)\boldsymbol{D}\right)\right]c_{j-\mathrm{int}(\beta-r_i/2-0\cdot5)-1}^{n}$$

$$+\left[\sum_{i=1}^{nqp}w_i\left(\frac{(1-r_i)(1+\upsilon_i)}{8}+\frac{(1-\alpha)\boldsymbol{D}}{2}\right)\right]c_{j-\mathrm{int}(\beta-r_i/2-0\cdot5)}^{n}$$

4P-LR2

$$\tfrac{1}{6}(c_{j-1}^{n+1}+4c_j^{n+1}+c_{j+1}^{n+1})-\alpha\boldsymbol{D}(c_{j-1}^{n+1}-2c_j^{n+1}+c_{j+1}^{n+1})$$

$$=\left[\left(-\frac{7}{360}\right)\frac{1-\upsilon}{2}\right]c_{j-\mathrm{int}\beta-3}^{n}+\left[\left(\frac{29}{180}-(1-\alpha)\boldsymbol{D}\right)\frac{1-\upsilon}{2}+\left(-\frac{7}{360}\right)\frac{1+\upsilon}{2}\right]c_{j-\mathrm{int}\beta-2}^{n}$$

$$+\left[\left(\frac{43}{60}+2(1-\alpha)\boldsymbol{D}\right)\frac{1-\upsilon}{2}+\left(\frac{29}{180}-(1-\alpha)\boldsymbol{D}\right)\frac{1+\upsilon}{2}\right]c_{j-\mathrm{int}\beta-1}^{n}$$

$$+\left[\left(\frac{43}{60}+2(1-\alpha)\boldsymbol{D}\right)\frac{1+\upsilon}{2}+\left(\frac{29}{180}-(1-\alpha)\boldsymbol{D}\right)\frac{1-\upsilon}{2}\right]c_{j-\mathrm{int}\beta}^{n}$$

$$+\left[\left(\frac{29}{180}-(1-\alpha)\boldsymbol{D}\right)\frac{1+\upsilon}{2}+\left(-\frac{7}{360}\right)\frac{1-\upsilon}{2}\right]c_{j-\mathrm{int}\beta+1}^{n}+\left[\left(-\frac{7}{360}\right)\frac{1+\upsilon}{2}\right]c_{j-\mathrm{int}\beta+2}^{n}$$

* υ, distance between node j and feet of characteristic lines in local co-ordinates (see Figure 1(a)).

advection is defined as (in local co-ordinates)

$$c^{\xi}(r) = \begin{cases} \dfrac{c_{\text{int}} - c_1}{r_{\text{int}} + 1} r + c_1 + \dfrac{c_{\text{int}} - c_1}{r_{\text{int}} + 1}, & r \in [-1, r_{\text{int}}], \\ \dfrac{c_{\text{int}} - c_2}{r_{\text{int}} - 1} r + c_2 - \dfrac{c_{\text{int}} - c_2}{r_{\text{int}} - 1}, & r \in [r_{\text{int}}, 1], \end{cases} \tag{24}$$

where c_{int} and r_{int} are respectively the concentration and location at time $n + 1$ of the forward-tracked node. The concentrations at the feet of the characteristic lines of the backward-tracked nodes, c_1 and c_2, are defined by linear polynomials.

The concept of piecewise integration fits efficiently into an ELLAM framework. In this framework there is not even the need for forward tracking. Indeed, the backward tracking which defines the weighting functions (Figure 2) allows integrals to be evaluated directly at time n and identifies unambiguously any relevant discontinuities within the domain of integration. Therefore fewer characteristic lines need to be tracked and an ELLAM implementation of the piecewise integration may be less expensive than its Galerkin FE-ELM counterpart. For constant coefficients the piecewise integration concept applied to each framework–Galerkin FE-ELM or ELLAM–leads to the same finite difference analogue (Table I).

Quadrature integration methods. The quadrature methods (qu-ELMs) evaluate the integrals at the feet of the characteristic lines by numerical integration.[17,18] In a Galerkin FE-ELM framework, quadrature points rather than nodes are backward tracked from $n + 1$ to n. Once the concentration and its first derivative at the feet of the characteristic lines of the quadrature points are interpolated, the evaluation of the integrals at time n becomes trivial:

$$\Phi_{kj}^{\xi} = \frac{2}{\Delta x} \int_{\Omega_k} (1 - \alpha) D \frac{\partial \phi_j}{\partial r} \frac{\partial c}{\partial r}\bigg|^{\xi} \mathrm{d}r = \frac{2(1 - \alpha) D}{\Delta x} \sum_{i=1}^{nqp} \chi_i \frac{\partial c_i}{\partial r}\bigg|^{\xi} \frac{\partial \phi_j}{\partial r}(r_i),$$

$$\Psi_{kj}^{\xi} = \frac{\Delta x}{2} \int_{\Omega_k} \phi_j \frac{c^{\xi}}{\Delta t} \mathrm{d}r = \frac{\Delta x}{2\Delta t} \sum_{i=1}^{nqp} \chi_i c_i^{\xi} \phi_j(r_i), \tag{25}$$

where c_i^{ξ} and $\partial c_i / \partial r|^{\xi}$ are respectively the concentration and its first derivative at the foot of the characteristic line for quadrature point i, r_i and χ_i are respectively the location (at time $n + 1$) and the weight of point i, $\phi_j(r_i)$ is the value of the weighting function at quadrature point i and nqp is the number of quadrature points. The finite difference analogue for a generic quadrature method is presented in Table I.

We selected the two quadrature integration methods that integrate exactly the highest-order polynomials: Gauss and Lobatto quadrature. For a given number of quadrature points, n, Gauss quadrature integrates exactly polynomials of order $2n$-1. While this order is lower for Lobatto quadrature ($2n$-3), this method includes the nodes as quadrature points and therefore can potentially lead to very different properties. The fact that the nodes are quadrature points has the additional advantage of reducing the tracking costs: in 1D only n-1 points per element need to be tracked. All the comparisons will therefore be performed between n Gauss points and $n + 1$ Lobatto points. In this way the two methods will be compared on an 'equal cost' as well as an 'equal order' basis.

Numerical integration can also be used in the context of ELLAMs, but, unlike for interpolation and piecewise integration, there is no direct correlation between integration Galerkin FE-ELMs and ELLAMs, even for constant coefficients. Indeed, in ELLAMs the role of numerical integration is specifically restricted to the evaluation of integrals, since the weighting function is defined through the backward tracking of nodes (not quadrature points). Because the quadrature in ELLAMs does not

dictate the number of characteristic lines to be tracked, ELLAMs may be less expensive than quadrature integration FE-ELMs (which in 1D usually require the tracking of three or more quadrature points for satisfactory accuracy).

4. STABILITY ANALYSIS

The stability of interpolation ELMs (including the 4P-LR2) was investigated earlier[2] and it was found that interpolation ELMs are unconditionally stable, except for cubic or higher-order compact interpolators and some Hermitian–Lagrangian interpolators. We therefore concentrate in this section on the stability of integration methods.

The analysis is primarily based on amplification factors and truncation errors. Amplification factors are used to examine the influence of the Courant number (β) and dimensionless wavelength ($L_m/\Delta x$), while truncation errors explain the influence of the diffusion number ($\boldsymbol{D}$). Targeted numerical experimentation, based on or influenced by the Convection–Diffusion forum,[30] illustrates some of the conclusions of the formal analysis. For additional numerical tests see Reference 31.

The exact solution of the advection–diffusion equation can be written as a summation of Fourier components:

$$c(x, t) = \sum_{m=-\infty}^{\infty} c_m(x, t) = \sum_{m=-\infty}^{\infty} A_m^n \exp\left(\mathrm{i}\,\frac{2\pi}{L_m}(x - ut)\right), \tag{26}$$

where $\mathrm{i} = \sqrt{(-1)}$, A_m^n are problem-related coefficients and L_m is the wavelength of the mth Fourier component. The error introduced by a numerical solution (G_m) on the concentration of the mth component can be defined as

$$G_m = \tilde{c}_m/c_m = |G_m| \exp(\mathrm{i}\varphi_m), \tag{27}$$

where c_m is the exact concentration, $\tilde{c}_m$ is the concentration given by the numerical algorithm, $|G_m|$ is the amplification factor and φ_m is the phase error.

The stability condition is

$$|G_m| < \exp(\boldsymbol{D}\lambda_m^2), \tag{28}$$

where

$$\lambda_m = 2\pi\Delta x/L_m. \tag{29}$$

Since all methods considered in this paper have linear core elements, the propagation errors are time-independent.[2] Therefore it is enough to analyse the amplification factors after a single time step. Contours of amplification factors for all selected ELMs (pure advection) are presented in Figures 3 and 4, with β ranging from 0 to 1 and $L_m/\Delta x$ from 2 to 34. The value of β was limited to a maximum of unity because the amplification factors *per time step* in ELMs with linear core elements depend only on the fractional part of β.[2,31]

Figures 3 and 4 show that the pi-ELM is unconditionally stable (Figure 3) while the qu-ELM is unstable for some ranges of β, for both Gauss and Lobatto quadratures. Figures 4(a)–4(c) show that different numbers and types of quadrature points lead to different patterns of conditional stability. Moreover, these figures suggest that the number of instability regions is related to the number of quadrature points. Indeed, each quadrature point (except when coinciding with a node) corresponds to a local maximum in a region of instability (Figure 5).

The instability of the qu-ELM can be eliminated by introducing a small amount of diffusion, which depends on both the type and number of quadrature points used. Since the maxima of the amplification factors decrease as the number of quadrature points increases (Figures 4 and 5), so will the amount of

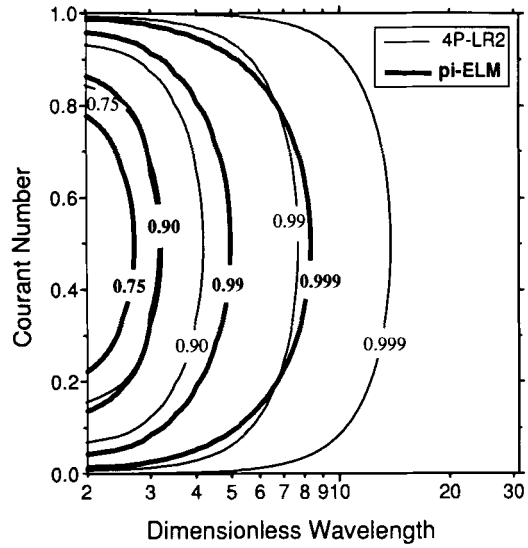

Figure 3. Amplification factor for pi-ELM and 4P-LR2 (pure advection)

diffusion necessary to guarantee stability. The use of a specific type of quadrature will also determine the value of $\boldsymbol{D}$ required for stability.

Truncation errors provide further insight to the influence of diffusion on stability and to the relationship between the instability regions and the quadrature points. It is convenient to define the

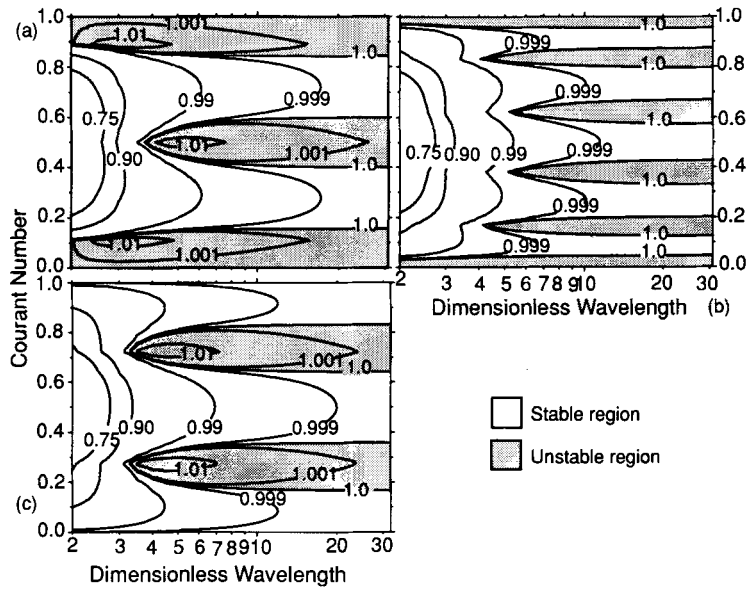

Figure 4. Amplification factor for qu-ELM (pure advection): (a) three Gauss points; (b) six Gauss points; (c) four Lobatto points

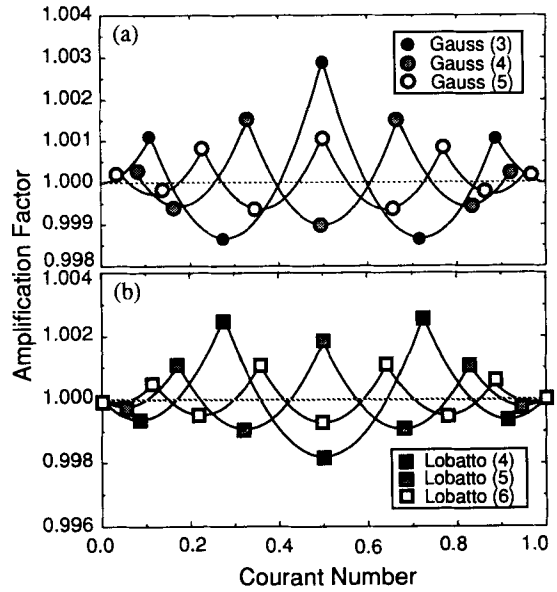

Figure 5. Comparison of amplification factors for qu-ELM with $L_m/\Delta x = 15$: (a) Gauss quadrature points; (b) Lobatto quadrature points

effective diffusion number (Υ) associated with the second derivative of concentration:

$$\Upsilon(\beta, \boldsymbol{D}) = \frac{\Delta t}{\Delta x^2}(D + \tau), \tag{30}$$

where τ is the numerical diffusion coefficient. A method will be stable for positive values of Υ and unstable otherwise. For the qu-ELM with a generic quadrature and a generic number of points we obtain (see Reference 31 for further details)

$$\Upsilon = \sum_{i=1}^{nqp} \left[\frac{w_i}{2}\left(\frac{2K_i^2+1}{4} - \frac{K_i \upsilon_i}{2}\right) - \frac{w_i r_i}{8}(2K_i - \upsilon_i)\right] - \left(\frac{\beta^2}{2} + \frac{1}{6}\right) + \boldsymbol{D}, \tag{31}$$

where υ_i is the distance between the left node and the foot of the characteristic line of point i in local co-ordinates $[-1, 1]$. K_i, which identifies the element that contains the foot of the characteristic line of each quadrature point, is defined as

$$K_i = \begin{cases} \text{int}\left(\beta - \dfrac{r_i}{2} - \dfrac{1}{2}\right) + 1 & \text{if } \beta - \dfrac{r_i}{2} - \dfrac{1}{2} > 0, \\ 0 & \text{otherwise.} \end{cases} \tag{32}$$

Contours of the effective diffusion number as a function of β and $\boldsymbol{D}$ are presented in Figures 6(a)–6(c) and confirm that the conditional stability of the qu-ELM can be eliminated by a very small amount of diffusion which depends on the number and type of quadrature points. The minimum diffusion number that leads to a positive effective diffusion was plotted against the number of quadrature points for both types of quadrature. Figure 7 shows that the minimum $\boldsymbol{D}$ decreases as the number of quadrature points increases for both types of quadrature points. The minimum diffusion numbers for n Gauss points and $n + 1$ Lobatto points are very similar.

Regardless of the type and number of quadrature points, the amount of diffusion required to stabilize qu-ELM is considerably smaller than the dispersion coefficients used in many numerical simulations. As an example, consider a 2D depth-averaged simulation with a spatial discretization of 100 m and a

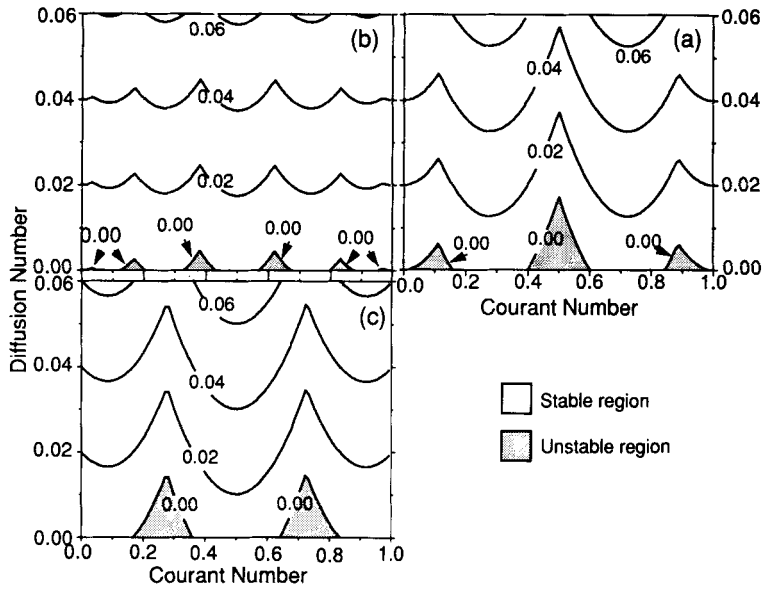

Figure 6. Truncation error—effective diffusion number for qu-ELM: (a) three Gauss points; (b) six Gauss points; (c) four Lobatto points

time step of 1800 s (representative values for coastal systems). A diffusion number of 0·02 is selected, which is enough to stabilize the qu-ELM with three or more Gauss points and four or more Lobatto points. This corresponds to a diffusion coefficient of 0·11 $m^2 s^{-1}$, which is well below the dispersion coefficients used in most depth-averaged simulations of surface water systems.[3,4]

However, problems may arise in three-dimensional simulations, since the vertical diffusion is

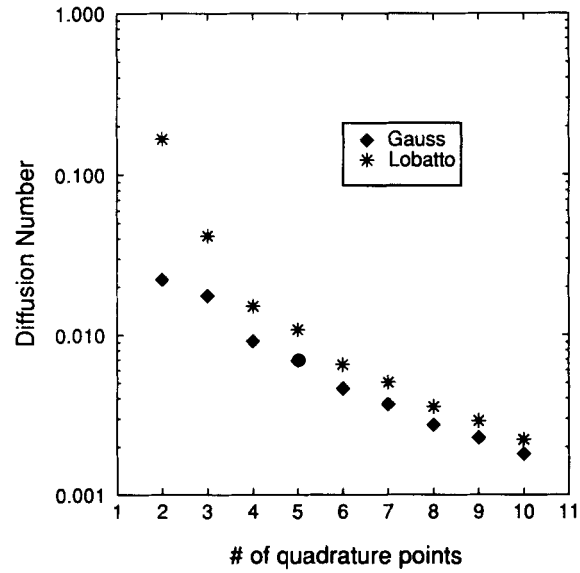

Figure 7. Minimum diffusion number required to stabilize qu-ELM as a function of type and number of quadrature points

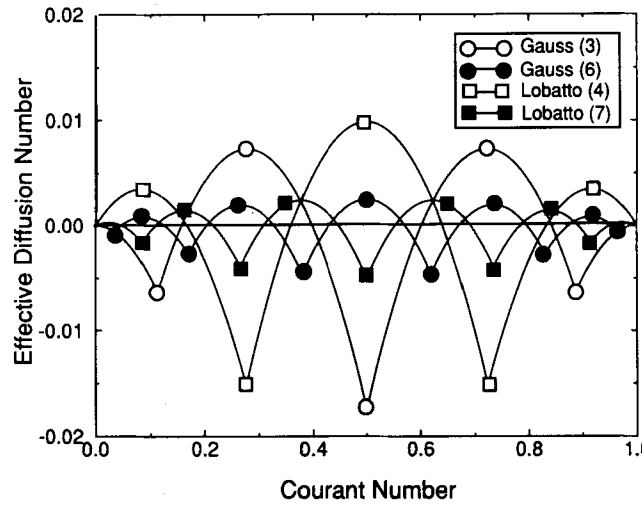

Figure 8. Comparison of effective diffusion numbers for alternative qu-ELM for $\boldsymbol{D} = 0$

considerably smaller than its horizontal counterparts. If we now consider a vertical discretization of 10 m for the same time step and diffusion number, a diffusion coefficient of $1{\cdot}1 \times 10^{-3}$ m^2 s^{-1} will result. Since the vertical diffusion coefficient is generally in the range 10^{-2}–10^{-5} m^2 s^{-1}, the minimum D required for stability is of the order of magnitude of or larger than the processes being modelled. A larger number of quadrature points can reduce the necessary numerical diffusion but would lead to an increasing computational cost. Therefore the use of quadrature integration methods in 3D may be restricted to particular cases.

Figures 6(a)–6(c) also confirm that the number of quadrature points is related to the number of instability zones. In order to analyse this relationship in further detail, Υ was plotted against β for $\boldsymbol{D} = 0$ for both Gauss and Lobatto quadratures (Figure 8). Results show that the number of local minima in Υ is equal to the number of quadrature points and that the first derivative of Υ is continuous everywhere except at the local minima. Since an instability region must include a local minimum, a discontinuity in the first derivative also identifies a *potentially* unstable region. Equations (31) and (32) show that these discontinuities are generated by unit steps in K_i when the foot of a characteristic line moves from one element to the next. A discontinuity will occur when K_i is increased by one for a Courant number given by (from (32))

$$\text{fractional}\left(\beta_i - \frac{r_i}{2} - 0{\cdot}5\right) = 0 \quad \Rightarrow \quad \beta_i = \frac{r_i}{2} + 0{\cdot}5 + z \quad (z \text{ integer}). \tag{33}$$

Therefore a minimum in Υ will occur when the foot of the characteristic line of any quadrature point coincides with a node.

Each type of quadrature will lead to a different relationship between the number of instability regions and the number of minima (and quadrature points), as suggested by the analysis of amplification factors. Lobatto points that coincide with nodes identify the integer Courant numbers only as minima, not as unstable zones (Figure 8). Since ELMs are exact for integer Courant numbers,[2] the Lobatto quadrature will have $nqp - 2$ unstable zones. Since all Gauss points are located in the interior of elements, the number of instability regions for Gauss quadrature coincides with the number of minima and with the number of quadrature points (Figure 8).

Table II· Numerical test parameters

Test	u (m/s^{-1})	D (m^2 s^{-1})	Type*	σ (m)	Δt (s)	Number of time steps	β	Initial condition	Up-stream BC	Down-stream BC
1	0·5	0	GH	264	192	50	0·48	$c_0(x) = \exp[-(x - x_0)^2/2\sigma_0^2]$†	$c = 0$	$c = c_{\text{advect}}$†
2	0·5	0	AF	—	96	100	0·24	$c_0 = 0$	$c = 1$	$c = c_{\text{advect}}$
3	0·5	0	GH	264	96	100	0·24	$c_0(x) = \exp[-(x - x_0)^2/2\sigma_0^2]$	$c = 0$	$c = c_{\text{advect}}$

* GH, Gauss hill; AF, advancing front.
† x_0, centre of mass; σ_0, standard deviation.
‡ c_{advect}, concentration after advective step.

In order to illustrate the properties previously established, two numerical tests were selected from the reference problems of the Convection–Diffusion forum.[30] In test 1 a Gauss hill is advected and diffused under a uniform flow. In test 2 the concentration field is imposed by a constant mass flux specified through the upstream concentration (advancing front). The parameters for all tests are presented in Table II. Concentrations are shown in Figures 9 and 10.

Results illustrate both the unconditional stability of the pi-ELM and the β-dependent stability of the qu-ELM identified earlier. For a β of 0·48 (Figure 9) the qu-ELM with three Gauss points is unstable while the qu-ELM with four Lobatto points presents a stable behaviour. A β of 0·24 provides stable solutions for Gauss quadrature, but the use of Lobatto points leads to an unstable result (Figure 10). When sharp, poorly discretized concentration gradients are present (Figure 10), both integration ELMs exhibit artificial oscillations that are not present in the reference solution. These oscillations have larger amplitude for the pi-ELM that for the qu-ELM, but they lead to the qu-ELM's instability when the fractional part of β falls in one of the unstable zones identified in our formal analysis (Figure 10). In a more general case of variable coefficients the qu-ELM may or may not lead to instabilities, depending on the specific distribution of Courant numbers in the domain.

The above results show that comparative study of methods can hardly be supported by numerical experimentation alone. The numerical experimentation can only simulate specific cases; therefore the global behaviour of methods with a strong dependence on one parameter cannot be well understood. Since the study of a method is traditionally based on a few tests only, an incorrect evaluation of the performance of the qu-ELM could result from an analysis based only on numerical experimentation.

5. ACCURACY ANALYSIS

The same tools used to investigate stability will now be used to characterize the accuracy of the selected interpolation and integration methods. While the simultaneous discussion of phase and amplification errors is in general recommended when studying accuracy, we concentrate here on the latter. This is appropriate because all methods of interest have rather small phase error,[31] an expected consequence of their linear core elements.[2]

All analysed interpolation and integration methods have rather good accuracy properties, as

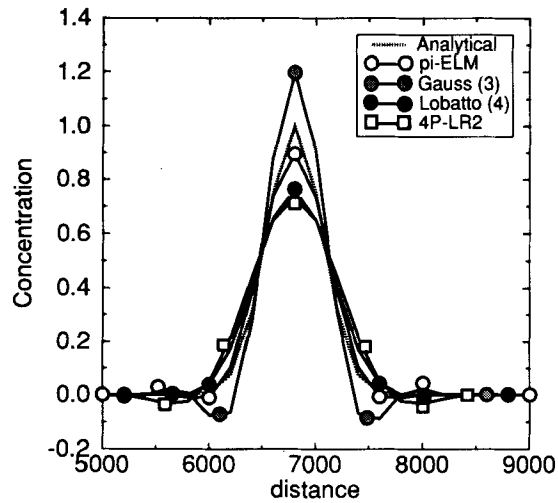

Figure 9. Concentration profiles for test 1

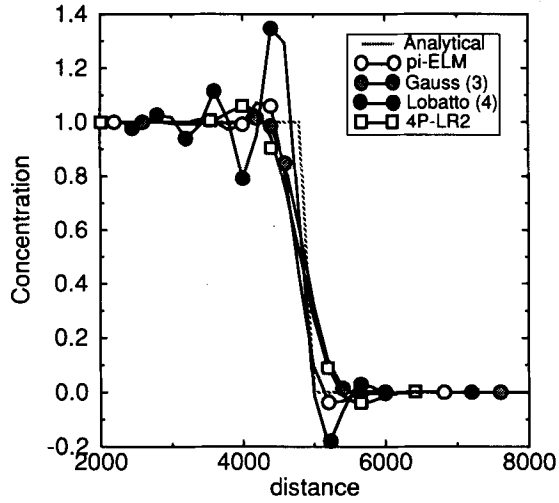

Figure 10. Concentration profiles for test 2

illustrated, for instance, by the relatively small number of dimensionless wavelengths required to bound the amplification error per time step to 1% (see Figures 3 and 4).

The accuracy of all methods clearly improves with increasing diffusion number and dimensionless wavelength, but accuracy dependence on the Courant number is less obvious. Errors per time step are fairly independent (strictly independent for amplification errors) of the integer part of the Courant number.[31] This a well-known characteristic of many ELMs[2] and is responsible for the unusually good performance of these methods for Courant numbers well above unity (when tracking is forced to be very accurate). Errors per time step do depend strongly, though, on the fractional part of the Courant number. This dependence is relatively smooth for the interpolation and piecewise integration methods but is rather complex, though predictable, for the quadrature integration method (Figures 5(a), 5(b) and 11).

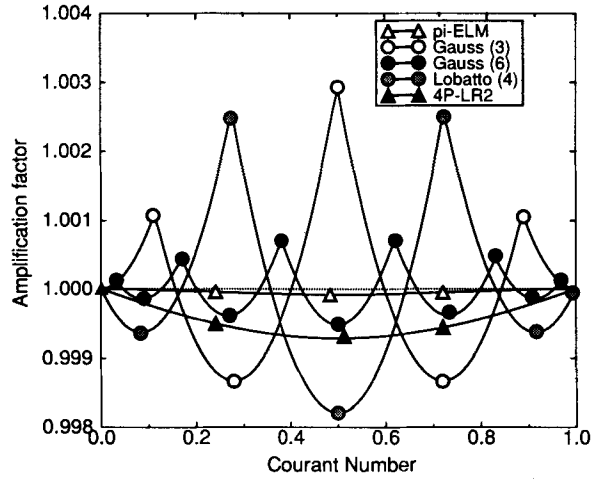

Figure 11. Comparison of amplification factors for $L_m/\Delta x = 15$: pi-ELM, qu-ELM and 4P-LR2

Figures 12(a) and 12(b) show statistics of the amplification factors after 100 time steps over the Courant number, as a function of $L_m/\Delta x$. Our primary objective is to show that while mean amplification factors (Figure 12(a)) may allow a quick comparison of accuracy and stability properties, they can mask some rather undesirable features. For instance, mean amplification factors suggest that the use of three Gauss points leads to excellent accuracy, tainted by very mild instability. Accounting for the variability of amplification factors over β, however, reveals very serious positive and negative diffusion and suggests that the method may frequently be unstable (Figure 12(b)). Furthermore,

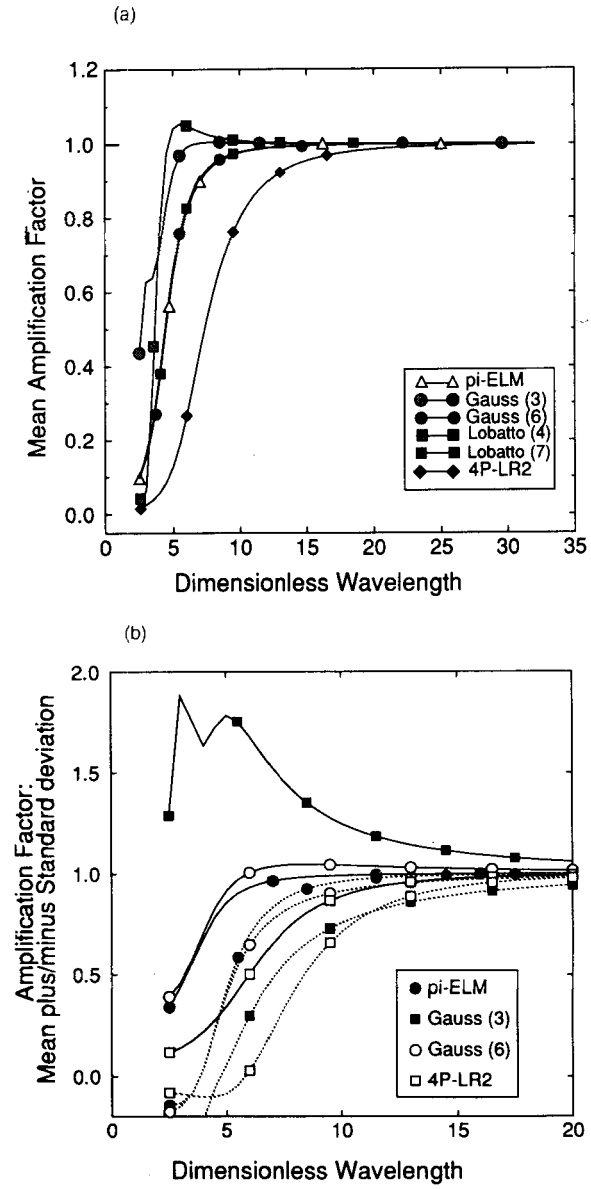

Figure 12. Comparison of amplification factor statistics after 100 time steps: (a) mean; (b) range limited by mean plus standard deviation (full curves) and mean minus standard deviation (dotted curves)

methods with wide standard deviations will, in the general case of varying coefficient transport, tend to significant numerical aliasing and associated mass imbalances.* Desirable properties are therefore mean amplification factors close to unity and standard deviations close to zero.

The accuracy of quadrature methods clearly increases with the number of quadrature points (Figure 5). It is difficult to compare the accuracy of *nqp* Gauss points and *nqp* + 1 Lobatto points for specific values of Courant number, since their stable regions do not overlap for most of the β-range (Figures 8 and 11). Their comparative performances for variable coefficient problems will depend on the specific distribution of β over the domain.

6. FINAL CONSIDERATIONS

Our analysis has concentrated on the stability and accuracy of a set of integration ELMs that are replacing more conventional interpolation Eulerian–Lagrangian formulations in environmental modelling. The added accuracy that the new methods can provide over interpolation techniques is illustrated in Figure 13 and is quite attractive. However, very few applications using integration ELMs have been reported and in general were limited to synthetic problems.[9,10] These methods still need to demonstrate that they can be applied effectively in multiple dimensions with unstructured grids, complex geometry and flows, and for problems involving multiple non-conservative tracers. The present paper does not directly address these issues but provides some basis for reflection.

1. Non-compact interpolation methods such as the 4P-LR2 enhance the accuracy of compact interpolation methods (for the same order of the core element), as shown by Baptista.[1,2] However, non-compact methods are cumbersome and arguably ambiguous to implement in multiple dimensions, except for simple grid patterns, and have not become the basis of any major finite element transport model. All other classes of methods analysed in this paper have the potential to lead to conceptually straightforward implementations in multiple dimensions.
2. The piecewise integration method arguably fares the best among all analysed methods. Indeed, amplification errors are among the smallest and the least sensitive to the fractional part of the Courant number and the method is not tainted by the spectre of conditional stability. Implementations of the 'exact' integration concept for complex multidimensional flows may, however, raise three important questions: (i) possible additional cost relative to the interpolation methods, due to the forward-tracking step; (ii) possible inability to preserve mass, much like interpolation methods, due to non-conservative flow fields, inaccurate tracking or boundary conditions; (iii) expensive, albeit conceptually straightforward, evaluation of integrals. The first and arguably part of the second of these questions may be addressed effectively if the piecewise integration concept is treated as a particular case of ELLAMs, although the extension of ELLAMs to multiple dimensions may bring additional problems.[22]
3. Quadrature integration methods have generally attractive accuracy properties, but their conditional stability prevents them from becoming a clearly preferred choice. Even if, arguably, many applications involve enough diffusion to stabilize the simulations, the strong dependence of accuracy on the fractional part of the Courant number is still to be regarded as a disadvantage and a likely source for aliasing and mass imbalances. In addition, quadrature methods required added tracking relative to interpolation methods.

ELLAMs can be perceived as a general framework in which either interpolation or piecewise integration concepts can be implemented. The extension of these concepts to multiple dimensions and

*For further details on the mechanism of generation of high-frequency noise see Reference 2.

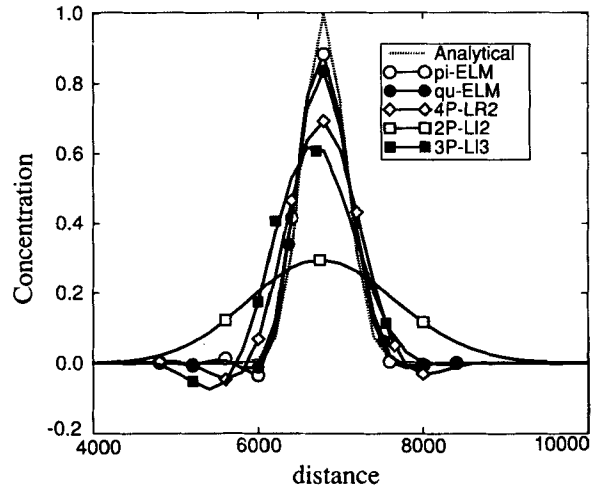

Figure 13. Concentration profiles for test 3: comparison of integration (pi-ELM and qu-ELM with six Gauss points) and interpolation (4P-LR2, linear interpolation (2P-LI2) and quadratic interpolator (3P-LI3)) ELMs

complex flows appears quite straightforward. It is therefore tempting to recommend that the development of ELLAMs and piecewise integration Galerkin ELMs be pursued in parallel in the future Eulerian–Lagrangian models for multi dimensional applications.

ACKNOWLEDGEMENTS

We thank André Fortunato for insightful discussions and suggestions and for critically reviewing earlier versions of this manuscript. We also thank Paul Turner for assistance with the software used to generate the figures. The first author was sponsored by Junta Nacional de Investigação Científica e Tecnológica (Portugal) under grants BM-1354/91-RN and BD-2775/93. The second author was partially supported by NSF grant ASC-8910805.

REFERENCES

1. A. M. Baptista, 'Accurate numerical modeling of advection-dominated transport of passive scalars: a contribution', Laboratório Nacional de Engenharia Civil, Lisbon, 1986.
2. A. M. Baptista, 'Solution of advection-dominated transport by Eulerian–Lagrangian methods using the backwards method of characteristics', *Ph.D. Dissertation*, Massachusetts Institute of Technology, Cambridge, MA, 1987.
3. A. M. Baptista, E. E. Adams and K. D. Stolzenbach, 'Eulerian–Lagrangian analysis of pollutant transport in shallow water', *Technical Report 296*, MIT R.M. Parsons Laboratory, Cambridge, MA, 1984.
4. J. D. Wang, S. V. Cofer-Shabica and J. Chin Fatt, 'Finite element characteristic advection model', *J. Hydraul. Eng., ASCE*, **114**, 1098–1114 (1988).
5. K. Dimou, '3-D hybrid Eulerian–Lagrangian/particle tracking model for simulating mass transport in coastal water bodies', *Ph.D. Dissertation*, Massachusetts Institute of Technology, Cambridge, MA, 1992.
6. M. F. Wheeler, K. R. Roberson and A. Chilakapati, 'Three-dimensional bioremediation modeling in heterogeneous porous media', *Proc. 9th Int. Conf. on Computational Methods in Water Resources*, Computational Mechanics Publ., Denver, CO, 1992.
7. L. R. Bentley and G. F. Pinder, 'Eulerian–Lagrangian solution of the vertically averaged groundwater transport equation', *Water Resources Res.*, **28**, 3011–3020 (1992).
8. T. M. Wood and A. M. Baptista, 'A model for diagnostic analysis of estuarine geochemistry', *Water Resources Res.*, **29**, 51–71 (1993).
9. P. Binning and M. A. Celia, 'Two-dimensional Eulerian–Lagrangian localized adjoint methods for the solution of the contaminant transport equation in the saturated and unsaturated zones', *Proc. 10th Int. Conf. on Computational Methods in Water Resources*, Kluwer, Dordrecht, 1994.

10. C. Cheng, G.-T. Yeh and T. E. Short, 'Modeling three-dimensional subsurface flow, fate and transport of microbes and chemicals (3DFATMIC)', *Proc. 10th Int. Conf. on Computational Methods in Water Resources*, Kluwer, Dordrecht, 1994.
11. R. Courant, E. Isaacson and M. Rees, 'On the solution of nonlinear hyperbolic differential equations by finite differences', *Commun. Pure Appl. Math.*, **5**, 243–255 (1952).
12. C. E. Leith, 'Numerical simulation of the Earth's atmosphere', *Methods Comput. Phys.*, **4**, 1–28 (1965).
13. O. Daubert, *Programme HYP1, Rapport C41/74/12*, Laboratoire National d'Hydraulique, Chatou, 1974.
14. S. P. Neuman, 'A Eulerian–Lagrangian numerical scheme for the dispersion–convection equation using conjugate space–time grids', *J. Comput. Phys.*, **41**, 270–294 (1981).
15. S. P. Neuman and S. Sorek, 'Eulerian–Lagrangian methods for advection–dispersion', *Finite Elements in Water Resources*, **4**, 14.41–14.68 (1982).
16. F. M. Holly and J. U. Polatera, 'Dispersion simulation in two-dimensional tidal flow', *J. Hydraul. Eng., ASCE*, **110**, 905–926 (1984).
17. Y. Hasbani, E. Livne and M. Bercovier, 'Finite elements and characteristics applied to advection–diffusion equations', *Comput. Fluids*, **11**, 71–83 (1983).
18. T. F. Russell, 'Time stepping along characteristic with incomplete iteration for a Galerkin approximation of miscible displacement in porous media', *SIAM J. Numer. Anal.*, **22**, 970–1013 (1985).
19. G. T. Yeh, J. R. Chang and T. E. Short, 'An exact peak capturing and oscillation-free scheme to solve advection–dispersion transport equations', *Water Resources Res.*, **28**, 2937–2951 (1992).
20. T. F. Russell, 'Eulerian–Lagrangian localized adjoint methods for advection-dominated problems', *Proc. 13th Bienn. Conf. on Numerical Analysis*, Pitman, Dundee, 1989.
21. M. A. Celia, T. F. Russell, I. Herrera and R. E. Ewing, 'An Eulerian–Lagrangian localized adjoint method for the advection–diffusion equation', *Adv. Water Resources*, **13**, 187–206 (1990).
22. M. A. Celia, 'Eulerian–Lagrangian localized adjoint methods for contaminant transport simulations', *Proc. 10th Int. Conf. on Computational Methods in Water Resources*, Kluwer, Dordrecht, 1994.
23. K. W. Morton, A. Priestley and E. Suli, 'Stability of the Lagrange–Galerkin method with non-exact integration', *Math. Modell. Numer. Anal.*, **22**, 625–653 (1988).
24. S. P. Neuman, 'Adaptive Eulerian–Lagrangian finite element method for advection–dispersion', *Int. j. numer. methods eng.*, **20**, 321–337 (1984).
25. S. Zisman, 'Simulation of contaminant transport in groundwater systems using Eulerian–Lagranian localized adjoint methods', *M.Sc. Thesis*, Massachusetts Institute of Technology, Cambridge, MA, 1990.
26. E. Varoglu and W. D. Liam-Finn, 'Utilization of the method of characteristics to solve accurately two-dimensional transport problems by finite elements', *Int. j. numer. methods fluids*, **2**, 173–184 (1982).
27. J. P. Benqué, G. Labadie and J. Ronat, 'A new finite element method for Navier–Stokes equations coupled with a temperature equation', *Proc. Fourth Int. Symp. on Finite Element Methods in Flow Problems*, North-Holland, Amsterdam, 1982, pp. 295–301.
28. A. Hauguel, 'Numerical modelling of complex industrial and environment flows', *Proc. Int. Symp. on Refined Flow Modelling and Turbulence Measurements*, vol. I, 1985.
29. J. M. Hervouet, 'Remarques sur la convection faible et son application à l'hydraulique', *Rapport HE41/86.09*, Laboratoire National D'Hydraulique, Chatou, 1986.
30. A. M. Baptista, E. E. Adams and P. Gresho, 'Benchmarks for the transport equation: the Convection–Diffusion forum and beyond', in Lynch *et al.* (eds.), *Quantitative Skill Assessment for Coastal Ocean Models*, AGU, 1994.
31. A. Oliveira, 'A comparison of Eulerian–Lagrangian methods for the solution of the transport equation', *M.Sc. Thesis*, Oregon Graduate Institute of Science & Technology, Portland, OR, 1994.
32. F. M. Holly and A. Preissmann, 'Accurate calculation of transport in two dimensions', *J. Hydraul. Div., ASCE*, **10**, 1259–1278 (1977).
33. J. Glass and W. Rodi, 'A higher order numerical scheme for scalar transport', *Comput. Methods Appl. Mech. Eng.*, **31**, 337–358 (1982).
34. J. Douglas Jr. and T. F. Russell, 'Numerical methods for convection–diffusion problems based on combining the method of characteristics with finite element or finite difference procedures', *SIAM J. Numer. Anal.*, **19**, 871–885 (1982).
35. O. Pironneau, 'On the transport–diffusion algorithm and its applications to the Navier–Stokes equations', *Numer. Math.*, **38**, 309–332 (1982).
36. R. T. Cheng, V. Casulli and S. N. Milford, 'Eulerian–Lagrangian solution of the convection–dispersion equation in natural coordinates', *Water Resources Res.*, **20**, 944–952 (1984).
37. P. J. Rasch and D. L. Williamson, 'On shape-preserving interpolation and semi-Lagrangian transport', *SIAM J. Sci. Stat. Comput.*, **11**, 656–687 (1990).
38. A. Staniforth and J. Côté, 'Semi-Lagrangian integration schemes for atmospheric models—a review', *Mon. Weather Rev.*, **119**, 2206–2223 (1991).
39. A. K. Ahsan and M. S. Bruno, 'Three-dimensional modeling of pollutant transport', *Proc. 2nd Int. Conf. on Estuarine and Coastal Modeling*, ASCE 1992.
40. P. Hansbo, 'The characteristic streamline diffusion method for convection–diffusion problems', *Comput. Methods Appl. Mech. Eng.*, **96**, 239–253 (1992).
41. C. Johnson, 'A new approach to algorithms for convection problems which are based on exact transport + projection', *Comput. Methods Appl. Mech. Eng.*, **100**, 45–62 (1992).